Journal of Membrane Science 718 (2025) 123700

Contents lists available at ScienceDirect

Journal of Membrane Science

journal homepage: www.elsevier.com/locate/memsci

Photocatalytic self-cleansing ZnO-coated ceramic membranes for preconcentrating microalgae

Amar K. Salih [a], Curtis P. Irvine [a], Fatima Matar [a], Lisa Aditya [b], Long D. Nghiem [b,**], Cuong Ton-That [a,*]

[a] School of Mathematical and Physical Sciences, University of Technology Sydney, Ultimo, New South Wales, 2007, Australia
[b] Centre for Technology in Water and Wastewater, School of Civil and Environmental Engineering, University of Technology Sydney, Ultimo, New South Wales, 2007, Australia

ARTICLE INFO

Keywords:
Microalgae harvesting
ZnO coating
Ceramic microfiltration membranes
Photocatalysis
Fouling control
Self-cleansing

ABSTRACT

Microalgae present strong potential for biofuel and bioproduct production; however, efficient harvesting methods remain a critical challenge to enhancing the economic competitiveness of microalgal products. This study introduces a simple approach for fabricating self-cleaning microfiltration membranes tailored for *Scenedesmus* sp. microalgae solutions by coating alumina substrates with ZnO. The ZnO layer was deposited using reactive magnetron sputtering and the functional properties of the membrane were tailored through controlled coating thicknesses. Surface characterization confirmed the formation of a uniform, crystalline ZnO layer. The solar light absorption of the ZnO-coated membrane was found to vary with coating thickness. The water contact angle of the membrane decreased from 80° to 42° after ZnO coating, demonstrating a substantial increase in hydrophilicity. While both uncoated and ZnO-coated alumina membranes initially exhibited a permeate flux of about 55 L m^{-2} h^{-1} (LMH), the ZnO-coated membranes demonstrated superior fouling resistance, with only a 5% flux decline after three filtration cycles compared to a 32% reduction in uncoated membranes. Under optimal conditions, the ZnO-coated membranes achieved full flux recovery within 30 min of solar simulator exposure, highlighting their excellent photocatalytic self-cleaning capabilities. The performance of the ZnO-coated membranes remained stable over three repetitive filtration cycles and membrane recovery, with the standard deviation of $< 5\%$, confirming the durability of the ZnO coatings. These findings highlight the potential of ZnO-coated ceramic membranes as a cost-effective solution for sustainable microalgae harvesting.

1. Introduction

Population growth and industrialisation have improved the world economy, but they have led to a significant increase in global energy and fuel consumption. A large body of research has focussed on the development of eco-friendly energy resources to reduce reliance on fossil fuels, secure access to fresh water and mitigate global warming [1,2]. Microalgae-derived biofuels and biochemicals have emerged as a sustainable alternative to fossil materials [3]. Microalgae are rich in proteins, carbohydrates, lipids, and nucleic acids, with lipid biomolecules such as fatty acids, triglycerides, phospholipids, and glycolipids offering a renewable source for the production of fuel and raw materials [4,5]. However, despite their potential, microalgae refineries have not been realized at industrial scale due to the high cost of harvesting [6,7]. Economically viable biofuel production requires efficient harvesting techniques that minimize energy and chemical consumption while enabling the recycling of water and nutrients [8]. There are currently no suitable harvesting techniques that satisfy both cost and environmental constraints for producing microalgae-derived biofuels and biochemicals [8,9].

Current microalgae harvesting techniques, such as centrifugation and chemical flocculation, are highly energy- and chemical-intensive, contributing significantly to the overall production cost. While centrifugation is effective and fast, it incurs high operational costs. Chemical flocculation, on the other hand, is less energy-intensive but requires flocculants like cationic polymers, which can increase maintenance requirements, complicate downstream processing and limit applications due to residual chemicals [10,11]. Recent research has demonstrated the

* Corresponding author.
** Corresponding author.
E-mail addresses: DucLong.Nghiem@uts.edu.au (L.D. Nghiem), Cuong.Ton-That@uts.edu.au (C. Ton-That).

https://doi.org/10.1016/j.memsci.2025.123700
Received 3 December 2024; Received in revised form 1 January 2025; Accepted 6 January 2025
Available online 6 January 2025

potential of microfiltration for preconcentrating microalgae for harvesting, improving biomass recovery efficiency and cost competitiveness [12,13]. However, previous studies also reveal that algal organic matter, consisting of extracellular and intracellular components, plays a dominant role in fouling by accumulating on the membrane surface and within pores, forming dense and irreversible fouling layers [14,15].

Several techniques, such as membrane vibration and frequent aerated backwashing, have been developed to tackle membrane fouling caused by high biomass levels [15,16]. Although these methods help restore membrane flux, the presence of thick extracellular polymeric materials from microalgae cells can lead to a gradual deterioration of the filtration process over time [15]. To mitigate membrane fouling effectively, incorporating and optimizing self-cleaning materials in microfiltration membranes is essential. Moreover, enhancing the membrane's wettability and introducing a surface charge can significantly reduce membrane fouling. Increasing hydrophilicity creates a hydration layer on the membrane surface, preventing direct contact between foulants and the membrane surface [17,18]. Additionally, electrostatic repulsion can inhibit foulants from attaching to the membrane surface, thereby reducing the fouling rate and improving filtration performance [19]. These techniques can alleviate but cannot completely remove fouling, and eventually membrane cleaning is still necessary.

Advanced oxidation processes (AOP) based on photoactive materials, such as TiO_2, ZrO_2, Fe_2O_3, ZnO, and MOF, have been explored in combination with membrane filtration to degrade and remove biocontaminants through the production of reactive oxygen species [20–23]. This approach provides a potential platform for developing self-cleansing membranes. When a semiconducting oxide material is illuminated with ultraviolet (UV) or solar light, electrons can be excited from the valence to the conduction band, generating free electron and holes. These electrons and holes can directly oxidize pollutants or interact with dissolved oxygen or OH^- ions in water to create reactive oxygen species (ROS), which degrade pollutants and organic foulants on the membrane surface [21]. Although photocatalytic degradation using metal oxides has been demonstrated for synthetic wastewater and organic compounds [24,25], few studies have investigated the use of coated membranes for microalgae harvesting, with membrane recovery rates of ~60% achieved after ultraviolet irradiation cleaning [26]. While surface coatings can enhance antifouling resistance and hydrophilicity, low-quality coatings may cause particle aggregation, significantly impairing its performance [27]. Deposition techniques such as electrospinning [28], dip coating [29], sol–gel [30], atomic layer deposition [24], and pulsed laser deposition [31], have been used for membrane coating; however, most methods encounter issues like non-uniformity, fragility, and limited membrane compatibility. In contrast, sputter deposition offers distinct advantages by providing strongly adherent, uniform coatings over large areas and accommodating porous membranes with irregular or curved surfaces [32]. ZnO is an effective photocatalyst for AOP, offering superior organic degradation compared to alternatives such as TiO_2 due to its higher electron mobility and a lower valence band position, which increases the oxidation potential of hydroxyl radicals [33,34]. Moreover, ZnO has low toxicity and is stable in aqueous environments at pH levels above 5 [35].

This study develops a self-cleaning membrane system to enhance microalgae biomass harvesting. We hypothesize that integrating a ZnO coating layer onto an alumina membrane will enable photocatalytic cleaning while reducing fouling through enhanced wettability. The approach involves incorporating a hydrophilic and photocatalytic ZnO coating onto a ceramic membrane. The ZnO layer was systematically characterized to confirm its photocatalytic functionality. The performance of the ZnO-coated membrane was evaluated for preconcentrating microalgae solutions, with key performance parameters including water permeability, and flux recovery through photocatalytic self-cleaning.

2. Materials and methods

2.1. Membrane preparation

A flat sheet ceramic membrane made of alumina (ALO) from Suzhou Dasen Electronic Material Co. (Jiangxi, China) was used. The membrane, measuring 150 mm by 100 mm, has an average pore size of 0.1 μm (according to the manufacturer). Before coating, the membrane was sequentially cleaned in an ultrasonic bath for 20 min using acetone, isopropanol and deionized water. After cleaning, it was dried with dry N_2 gas and stored in an airtight container. During deposition, the membrane was placed on a rotating stage approximately 10 cm from the sputtering target in a sputtering chamber, as described previously [26]. ZnO layers of varying thicknesses (200, 450, 750, and 1100 nm, denoted as T–ZnO/ALO, where T is the coating thickness) were deposited onto the membrane using direct current reactive sputtering (plasma power of 100 W) from a Zn target in a gas mixture of Ar and O_2 with a ratio of 3:1. The thickness of the ZnO coating was monitored by a quartz crystal thickness monitor. Post-deposition, the ZnO-coated membranes were annealed in ambient air at 500 °C for 2 h to improve the crystallinity of the ZnO layer. The uncoated membrane was also annealed under identical conditions and used as a control sample. Additionally, a glass slide was placed beside the membrane during deposition to obtain a ZnO film of identical thickness for optical analysis.

2.2. Membrane characterization

The ZnO-coated and uncoated ceramic membranes were characterized to evaluate their coating thickness, surface morphology, composition, crystallinity, and hydrophilic properties. X-ray diffraction (XRD) analysis was conducted using a Bruker D8 Discovery diffractometer with Cu Kα radiation. Optical absorption measurements were measured using an Agilent Cary 7000 UV–Vis spectrometer. The coating thickness was determined using a Bruker DektakXT profilometer, while hydrophilicity and contact angles were measured using an Attension optical tensiometer. Surface morphologies of the membranes were investigated with a Zeiss Supra 55VP field emission scanning electron microscope (SEM) equipped with Oxford Instruments Energy Dispersive Spectrometer (EDS). SEM images were analysed using ImageJ software to determine membrane pore sizes. The membrane surface roughness was measured using Park XE7 atomic force microscopy (AFM). X-ray photoelectron spectroscopy (XPS) data were collected at the Australian Synchrotron's Soft X-ray Spectroscopy (SXS) beamline.

2.3. Membrane filtration performance

The uncoated ALO and ZnO/ALO membranes were utilized in a submerged configuration (Fig. 1a). A plate and frame membrane module was submerged in a rectangular glass reservoir with dimensions of 45 cm in height, 20 cm in length, and 5 cm in width. A Masterflex Peristaltic pump (Cole-Parmer) was used to facilitate the clean water extraction from the membrane module. The system contained a digital pressure gauge data logger (Pressure Meter SDL700) to monitor the transmembrane pressure (TMP). Permeate water was collected in a storage tank, while water flux was measured using a digital balance (PGL 8001).

2.3.1. Effects of the ZnO coating on filtration performance

The effects of the ZnO coating on the ceramic alumina membrane were investigated by measuring the TMP at a flow rate of 30 mL/min and the rejection rate of a microalgae solution for both coated and uncoated ALO membranes. The initial volume of the microalgae solution was 4.5 L, while each filtration cycle was set to recover 1 L of water. All filtration experiments were conducted in duplicate to ensure reproducibility and calculate uncertainty. Before each replicate measurement, the membranes were backwashed at a flow rate of 30 mL/min for 3 min to remove the cake fouling layer, followed by rinsing with tap water, 30

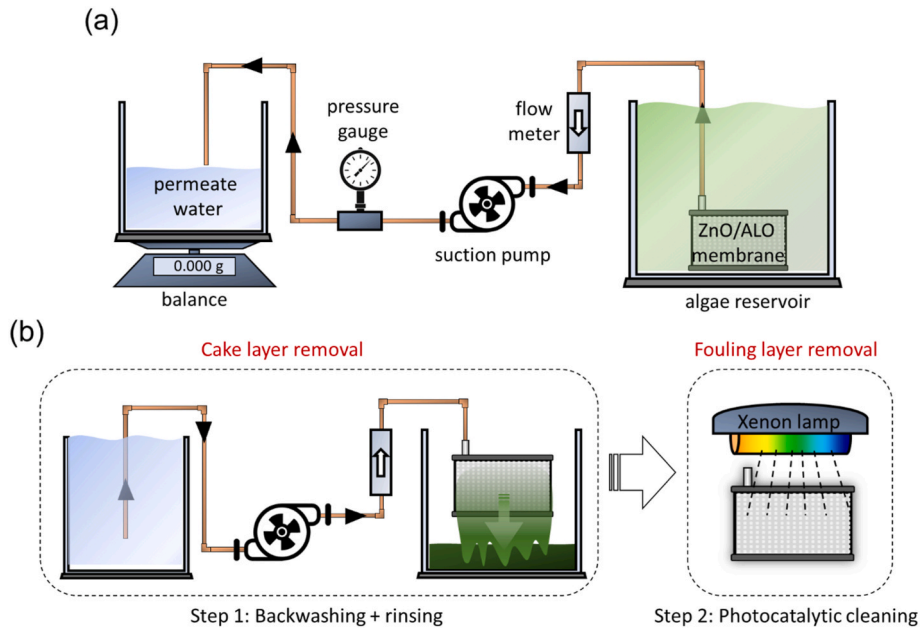

Fig. 1. (a) Schematic diagram of the membrane filtration system, which includes a submerged membrane module, algae reservoir, flow meter, suction pump, pressure gauge, balance, and storage tank. (b) Schematic diagram of the cleaning protocol for the ZnO/ALO membrane. Step 1 entails backwashing and rinsing the membrane with permeate water to remove the cake fouling layer, followed by Step 2, which involves photocatalytic cleaning using solar irradiation.

min of sonication in isopropyl alcohol (IPA), and 15 min of sonication in Milli-Q water. The flux (J), rejection rate (R), and flux recovery rate (FRR) are calculated by the following equations:

$$J\,(LMH) = \frac{V}{At} \quad \text{(Eq. 1)}$$

$$R\,(\%) = \left(1 - \frac{C_p}{C_f}\right) \times 100\% \quad \text{(Eq. 2)}$$

$$FRR\,(\%) = \left(\frac{J_c}{J_o}\right) \times 100\% \quad \text{(Eq. 3)}$$

where V is the volume of filtered water, A is the effective filtration area, t is the filtration time, C_f and C_p are the concentrations of the feed solution and permeate solution, respectively, both measured using optical density at 680 nm (OD_{680nm}). J_c and J_o are the flux of the cleaned and original membranes, respectively. The filtration performance of the membrane was also evaluated over three repetitive filtration cycles. After each cycle, the membrane was kept inside the algae reservoir and backwashed at a flow rate of 30 mL/min for 3 min before starting the subsequent cycle. The TMP was monitored and recorded every minute during each filtration cycle. To investigate the effect of aeration on the permeate flux, a plastic tube connected to an air pump was placed at the bottom of the reservoir to deliver an airflow of 0.5 LPM (litre per minute) when required.

2.3.2. Recovery of ZnO/ALO membranes by photocatalysis

Milli-Q water was used to determine the initial clean water flux for ALO and ZnO/ALO membranes. To form a fouling layer, 1 L of the microalgae solution was filtered through the membrane at a flow rate of 30 mL/min. Two cleaning steps were performed to recover the membrane flux (Fig. 1b) and the recovery rate was examined after each step. The first step involved backwashing the membrane with permeated water to remove the cake layer deposited during filtration. The second step involved removing the membrane module and rinsing it with tap water to remove any remaining cake layer. Next, the membrane was placed inside a container and submerged in water with the water level maintained at approximately 1 cm above the membrane to minimize light scattering. The membrane was then exposed to a solar simulator for 30 min. The solar simulator used was a 300 W xenon lamp (Perfect Light, PLS-SXE 300) with a wavelength range of 320–780 nm and the light intensity was 100 mW/cm^2 (1 Sun). Long-term filtration performance of the alumina and ZnO/ALO membranes was examined using 3 L of the microalgae solution over three repetitive filtration cycles (1 L in each cycle).

2.4. Microalgae

The green microalgae strain *Scenedesmus* sp. (UTS-LD), isolated in Australia by the University of Technology Sydney (UTS), was used in this study. *Scenedesmus* sp. typically forms clusters of four cells known as a coenobium, with each coenobium resembling a comb shape approximately 12 μm long and 3–5 μm wide. The cells of *Scenedesmus* sp. exhibit a zeta potential of −23.2 ± 1.3 mV. The culture was maintained at the UTS Algae Production Facility using MLA medium and grown under laboratory conditions in pilot-scale photobioreactors ranging from 120 to 350 L, as described in a previous study [7]. For all measurements, the microalgae solution was kept at a concentration of 1.5 OD_{680nm}, corresponding to 0.7 mg/mL for *Scenedesmus* sp.

3. Results and discussions

3.1. Structural properties of the neat alumina and ZnO/ALO membranes

Preliminary work was conducted to optimize the deposition time for desirable ZnO coating thickness. To validate the results, ZnO was initially coated on a flat glass slide at specific deposition times and the coating thickness was measured using a profilometer [36], as shown in Fig. S1(a). The results confirmed successful deposition with average thicknesses of 200 ± 5 nm, 450 ± 5 nm, 750 ± 5 nm, and 1100 ± 5 nm. For clarity, these membranes are labelled as 200 nm–ZnO/ALO, 450 nm–ZnO/ALO, 750 nm–ZnO/ALO, and 1100 nm–ZnO/ALO, respectively.

SEM imaging reveals that the neat (uncoated) alumina membrane has a rough surface whereas the ZnO coated membranes show micron-sized ZnO domains with lateral dimensions of 1–3 μm (Fig. 2a). The

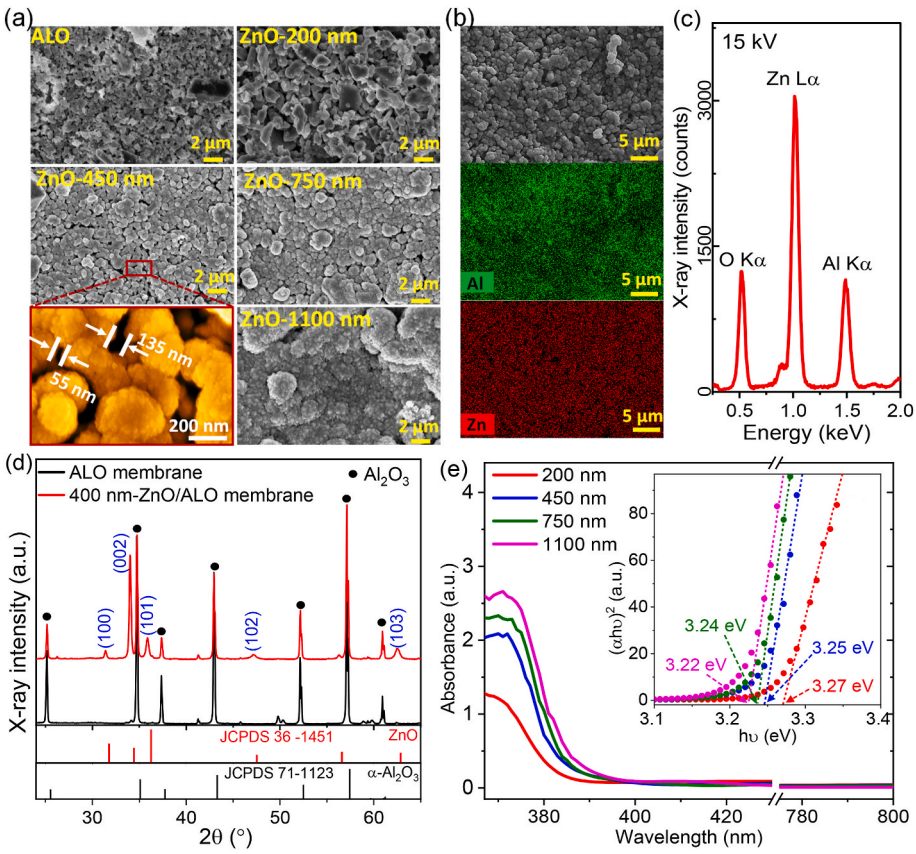

Fig. 2. (a) SEM images of the neat alumina and ZnO-coated membranes with ZnO layer thicknesses of 200, 450, 750 and 1100 nm. (b, c) EDX elemental maps and spectrum of the 450 nm thick ZnO/ALO membrane acquired at 15 kV, showing a homogenous ZnO coating even over the membrane pores. (d) XRD patterns of neat alumina and 450 nm-ZnO/ALO membranes. (e) UV–Vis absorption spectra and Tauc's plots for the ZnO coating layers, yielding the optical bandgap values indicated within the graph.

uncoated alumina membrane exhibits non-uniform pores characteristic of porous ceramic membranes [24]. For the 200 nm-ZnO/ALO membrane, near-complete coverage by ZnO is observed with small visible gaps between ZnO domains. In contrast, the ZnO/ALO membranes with ZnO thicknesses of 450 nm and above show a continuous ZnO coating layer on the alumina substrate, while maintaining sufficient pore size to allow the passage of water. The average pore size of the ALO membrane is ~100 nm. Coating the membrane with ZnO layers of 200 nm, 450 nm, 750 nm, and 1100 nm in thickness results in an average pore size reduction of ~36%, 65%, 71%, and 92%, respectively. EDX elemental maps of Al and Zn as well as the EDX spectrum of the 450 nm-ZnO/ALO membranes (Fig. 2b and c) reveal complete coverage of the membrane surface by ZnO, even over the membrane pores, demonstrating the effectiveness of the reactive sputtering technique and rotating stage during deposition. At the acceleration voltage of 15 kV, the electron beam penetrates the ZnO coating down to the alumina membrane, resulting in a uniform Al elemental EDX map (Fig. 2b). Coating the membrane with a 450 nm-thick ZnO layer reduces its surface roughness from 372 nm to 195 nm [Fig. S1(b)]. However, thicker ZnO coatings (750 nm and 1100 nm) lead to vertical grain growth (Fig. 2a), causing the surface roughness to exceed the measurement limit of the AFM. These results suggest a ZnO coating thickness of 450 nm is optimal as it effectively covers the membrane surface while minimizing surface roughness. The XRD patterns for the membranes (Fig. 2d), exhibit diffraction peaks (marked with black dots) attributed the α-Al_2O_3 phase of the alumina substrate [37], and the hexagonal wurtzite structure of ZnO layer, with diffraction peaks indexed to the (100), (002), (101), (102), (110), and (103) planes (JCPDS 36–1451) [26]. The optical absorption spectra of the ZnO coating layer (Fig. 2e) reveal a higher absorbance and a red shift in the absorption edge with increasing layer thickness. Tauc plot analysis of the ZnO layers (inset of Fig. 2e) shows a slight decrease in the band gap from 3.27 to 3.22 eV as the ZnO thickness increases from 200 to 1100 nm. This decrease in the optical bandgap with increasing film thickness is consistent with previous results of ZnO film growth by sputter deposition and is attributed to larger grain sizes and higher crystalline quality with increasing film thickness [38].

3.2. *Membrane hydrophilicity*

Surface hydrophilicity of the alumina and ZnO/ALO membranes is reported as water contact angle in Fig. 3). The contact angle of the alumina membrane is approximately 80°, consistent with previously reported values for alumina membranes [39]. Upon coating with ZnO, the contact angle decreases to 42 ± 4° for ZnO coating thicknesses between 200 and 750 nm, indicating an increase in the hydrophilicity of the coated membranes due to the hydrophilic nature of ZnO. This enhancement in hydrophilicity can be attributed to the presence of –OH groups on the ZnO surface, which interact with water molecules [26]. Furthermore, the contact angle of the 1100 nm–ZnO/ALO further decreases to 30°, likely due to the increased surface roughness of the thicker coating (Fig. 3a; ZnO-1100 nm). This observation is consistent with Wenzel's model, which states that increased surface roughness enhances the contact area between a droplet and the film surface, thereby increasing wettability [40]. Surface analysis of the oxygen chemical state in the alumina and ZnO/ALO coatings is analysed using XPS, with a photon energy of 650 eV (corresponding to a sampling depth of ~2 nm) (Fig. S2). Deconvolution of the O 1s spectra reveals two fitted peaks corresponding to two different chemical states of oxygen: O^{2-} ions (O–Zn) in the fully coordinated ZnO at a binding energy of 530.6 eV, and surface hydroxyl groups (Zn–OH) at 532.4 eV [41,42]. The OH/O–Zn

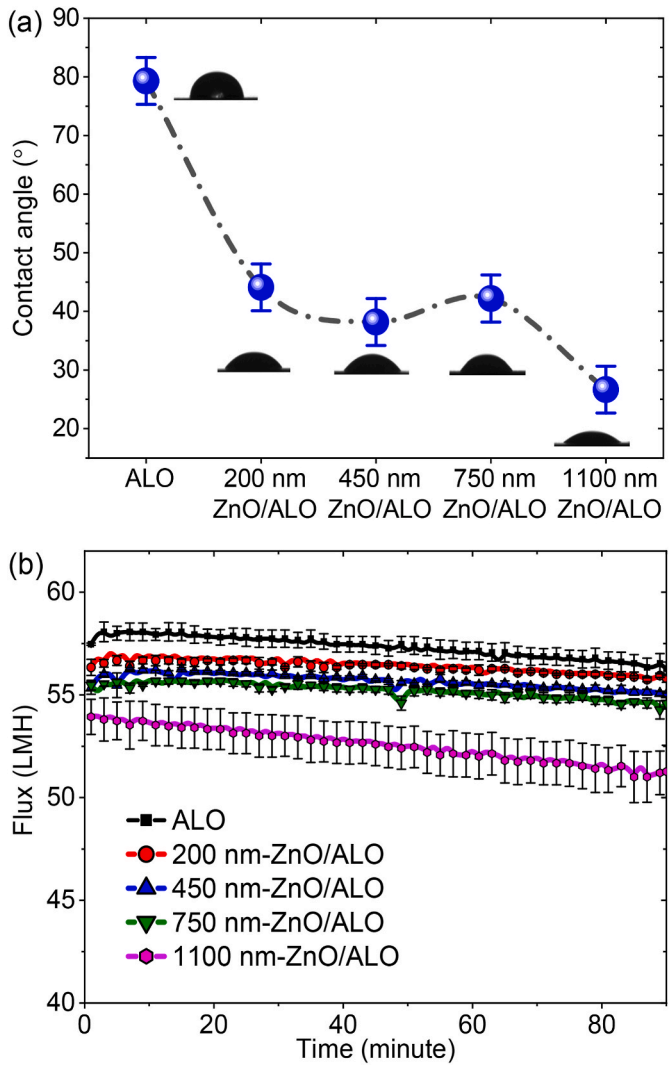

Fig. 3. (a) Contact angle measurements for the ALO and ZnO/ALO membranes, accompanied by the photo of the water droplet on the membrane surface. (b) Pure water flux through the neat alumina and ZnO/ALO membranes. Error bars represent the standard deviation calculated from two measurements.

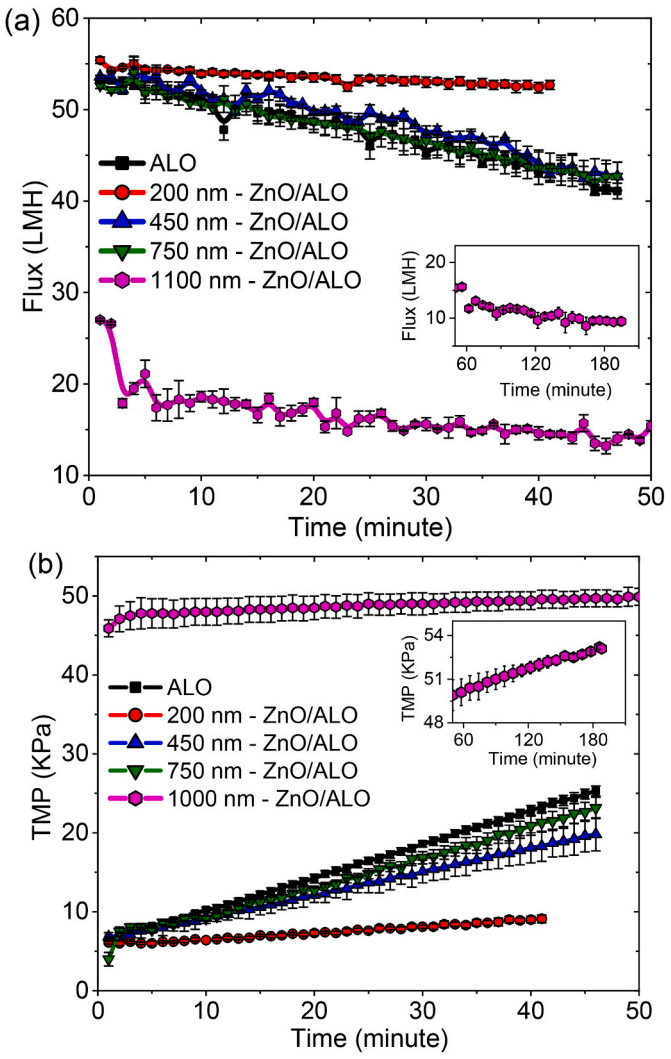

Fig. 4. Variations of (a) flux, (b) TMP of the neat ALO and ZnO-coated ALO membranes during the filtration of 1 L of microalgae solution under non-aerated filtration conditions. The insets display the performance of the 1100 nm–ZnO/ALO membrane over extended filtration cycles. The error bar represents the standard deviation from two measurements.

peak intensity ratio is found to be 0.24 for the neat alumina and 0.62 for the 450 nm-ZnO/ALO, indicating a higher proportion of surface –OH groups in the coated membranes.

The uncoated alumina membrane exhibits a water permeate flux of around 58 LMH (Fig. 3b). Remarkably, all ZnO/ALO membranes show no significant flux reduction despite the decrease in pore size caused by the ZnO coatings, except for the membrane with a ZnO coating thickness of 1100 nm. This suggests that the increased hydrophilicity provided by the ZnO coating compensates for the reduced pore size, maintaining consistent water permeate flux. This observation, consistent with previous studies [25], indicates that coating ceramic membranes with hydrophilic metal oxide layers can sustain permeate flux even as pore size decreases. The permeate flux remains stable across all ZnO-coated membranes over the 90-min filtration period.

3.3. Microalgae filtration performance

ZnO coating improves the filtration performance considerably. A volume of 1 L of pre-concentrated *Scenedesmus* sp. microalgae solution with an initial biomass concentration of 0.7 g/L was used to test the filtration performance of the alumina and ZnO/ALO membranes (Fig. 4a). The uncoated alumina membrane as well as the 450 nm–ZnO/ALO, and 750 nm–ZnO/ALO membranes also show a similar filtration profile. It took approximately 50 min to complete one filtration cycle (1 L) for each of the membranes. The decrease in permeate flux over time for the three membranes is due to the accumulation of microalgae on the membrane surface. The fouling rate is significantly less for the 200 nm–ZnO/ALO membrane, which has a shorter filtration cycle of 40 min. This improvement in filtration performance could be attributed to the combined effects of a relatively larger pore size and the hydrophilic ZnO-coated layer [24]. However, the 1100 nm–ZnO/ALO membrane exhibits an immediate drop in permeate flux, followed by a continued decline over a longer filtration cycle (Fig. 4a inset). The increase in TMP caused by the membrane's pore blockage is shown in Fig. 4b. Except for the 1100 nm-ZnO/ALO membrane, all the ZnO/ALO membranes exhibit lower TMP at the end of the filtration cycle than the uncoated alumina membrane. This is due to the more hydrophilic coating layer possibly due to the presence of hydroxylic groups on ZnO surface (Fig. S2). At the end of the filtration cycle, the TMP for the 200 nm–ZnO/ALO membrane is around 10 kPa, followed by 20 kPa, 23 kPa, and 53 kPa for the 450 nm, 750 nm and 1100 nm–ZnO/ALO membranes, respectively, approximately proportional to the increase in the thickness of the coating layer.

Scenedesmus sp. has a cylindrical-fusiform shape and exists as a

coenobium consisting of four cells, each larger than 10 μm [15]. This size prevents it from passing through or fully covering the pores, causing it to adhere to the membrane surface. As expected, the measured microalgae rejection by the neat alumina and ZnO/ALO membranes was all above 99.9%. Aeration effectively reduces membrane fouling (Fig. S3). Under the aeration filtration condition, both the uncoated ALO and 450 nm–ZnO/ALO membranes exhibit a significant increase in permeate flux rate and reduction in TMP. This improvement in filtration performance is attributed to the synergistic effects of buoyancy and drag force from flowing bubbles, which reduce fouling by the dense cell cake layer.

3.4. Multi-filtration cycle performance

The long-term filtration performance of the alumina and ZnO/ALO membranes was evaluated over three repetitive filtration cycles. After each cycle, the membranes were backwashed at a flow rate of 30 mL/min for 3 min. A notable drop in permeate flux and an increase in TMP were observable after each filtration cycle for the uncoated alumina membrane (Fig. 5a). At the end of the second cycle, the permeate flux decreased by approximately 25% compared to the end of the first cycle, and this reduction further increased to 34% after the third cycle. The TMP increased by 32% after the first cycle and by an additional 16% after the second cycle. The decline in filtration performance is caused by the accumulation of *Scenedesmus* sp. on the membrane despite backwashing after each cycle. Conversely, the electrostatic repulsion between the negatively charged ZnO/ALO membrane surfaces due to the surface –OH groups and negatively charged *Scenedesmus* sp. cells (zeta potential of -23.2 ± 1.3 mV) reduces the adhesion of algae cells to the membrane wall, making the backwashing process more efficacious [43]. For instance, the 200 nm–ZnO/ALO membrane (Fig. 5b) exhibits only a 5% decrease in flux and less than a 24% increase in TMP after each cycle. Similar behaviour was observed for the 450 nm–ZnO/ALO and 750 nm–ZnO/ALO membranes (Fig. 5c and d). However, the smaller pore size in these two membranes results in a noticeable drop in permeate flux and an increase in TMP, although their filtration performance is still better than the uncoated alumina membrane. In the case of the 1100 nm–ZnO/ALO membrane, significantly small pore sizes led to the formation of multiple leakage spots at the membrane terminals due to excessive TMP during backwashing step, which limits the possibility of reusing this membrane in other experiments.

3.5. Self-cleansing performance of the ZnO/ALO membranes

The self-cleaning property of the alumina and ZnO/ALO membranes is demonstrated in Fig. 6. The permeate water flux for the fouled membranes was recorded after backwashing and after irradiation with a solar simulator, and then compared with the initial unfouled membrane flux (Fig. 6a). The neat alumina membrane recovers around 68% of its initial permeate flux after backwashing and around 81% after 30 min of solar irradiation. The slight improvement in the uncoated alumina is due to its ability to absorb a portion of the UV light from the solar irradiation [44,45]. No further flux increase is observed with longer irradiation. In contrast, the ZnO/ALO membranes show a noticeable improvement in flux recovery after solar light irradiation, confirming the self-cleaning properties of the ZnO-coated layers. The 450 nm–ZnO/ALO membrane shows a flux recovery rate of 82% after the backwashing step and 102% after light irradiation. Slightly lower filtration performance was observed in the case of the 750 nm–ZnO/ALO membrane, with flux recovery rates of 79% and 98% after the backwashing and light irradiation steps, respectively. The slight reduction in recovered flux can be attributed to the blockage of some pores, likely caused by the higher TMP resulting from the decreased pore size in the 750 nm–ZnO/ALO membrane, as shown in Fig. 5d. Although the 200 nm–ZnO/ALO membrane shows the highest recovery rate through the backwashing process (83%), only around 90% flux recovery rate is achieved after light irradiation, indicating a lower photocatalytic self-cleaning property compared to the ZnO/ALO membranes with thicker ZnO coatings. This is likely due to the lower solar absorbance of the 200 nm–ZnO/ALO (Fig. 2e), which leads to a reduced generation of photogenerated radicals, limiting the oxidation of the deposited organic compounds [46,47]. Among the ZnO-coated membranes, the 450 nm–ZnO/ALO membrane

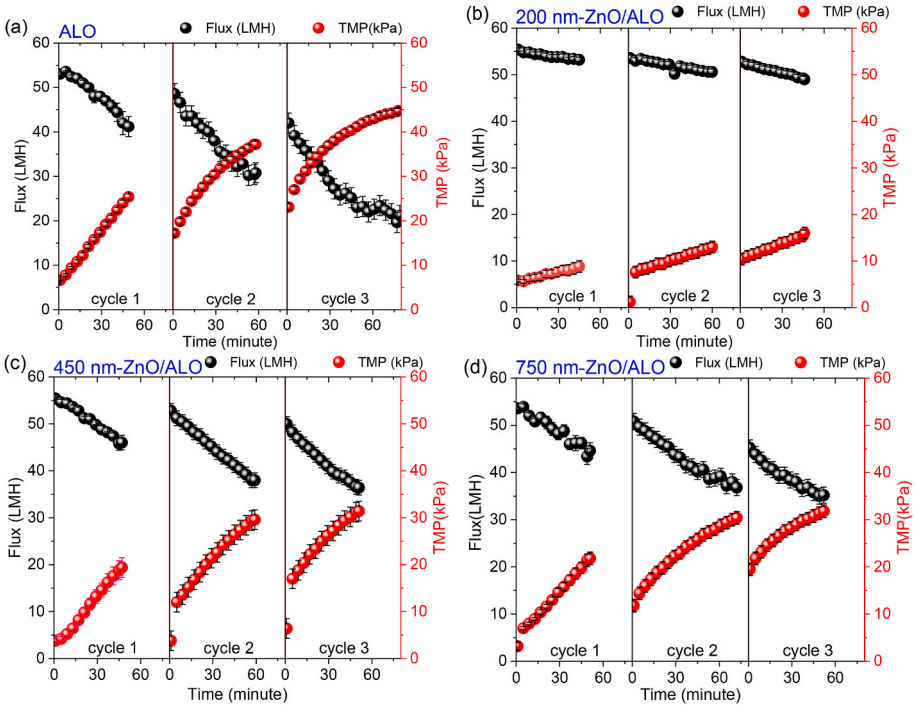

Fig. 5. Comparison of permeate flux and TMP of (a) ALO, (b) 200 nm–ZnO/ALO, (c) 450 nm–ZnO/ALO, and (d) 750 nm–ZnO/ALO membranes during the dewatering of the microalgae solution across three repetitive filtration cycles. Each cycle involves recovering 1 L of water, followed by backwashing for 3 min. The error bars in the second and third cycles has been estimated from the first cycle.

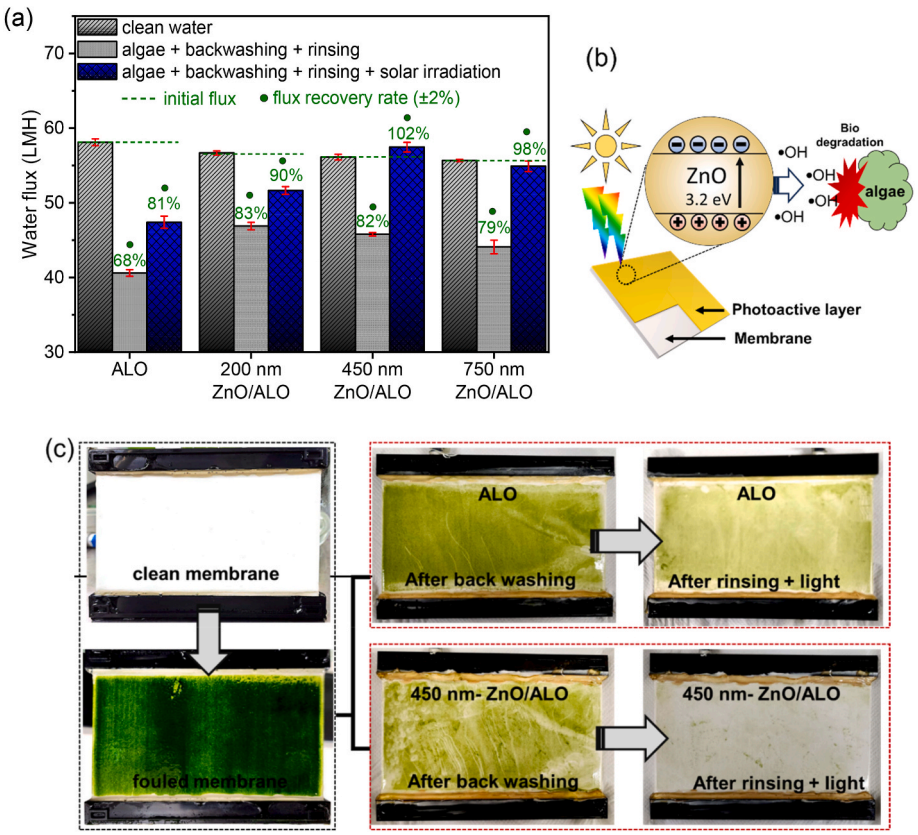

Fig. 6. (a) Permeate water flux of the neat alumina and 450 nm–ZnO/ALO membranes under three conditions: (i) before fouling, (ii) after fouling and cleaning with backwashing (BW) and rinsing, and (iii) after fouling and cleaning with BW, rinsing and solar light irradiation. Error bars represent the standard deviation from two replicate experiments. (b) Schematic diagram illustrating the self-cleansing capability of photocatalytic ZnO/ALO membranes. (c) Optical images of the fouled alumina and 450 nm–ZnO/ALO membranes before and after backwashing, followed by solar light cleansing.

demonstrates the best performance, with comparable initial flux to that of the uncoated, 200 nm– and 750 nm–ZnO/ALO-coated membranes, and highest self-cleaning properties among all the membranes. Notably, prolonging the backwashing step does not significantly enhance the removal of biofouling. The self-cleaning mechanism of ZnO-coated membranes under solar light irradiation is illustrated in Fig. 6b. The simulated solar light used in this test has a wavelength range of 320–780 nm (corresponding to photon energies of 3.9–1.6 eV), which is partly absorbed by the ZnO coating layer (3.2 eV). Upon irradiation, the ZnO coating generates free electrons and holes, triggering photocatalytic activity. The photogenerated holes are effective at oxidizing organic compounds through the generation of ROS, including superoxide ($O_2^{-\bullet}$), peroxide (O_2^{2-}), and hydroxyl radicals ($OH^{\bullet}$). These reactive species effectively degrade organic materials such as microalgae residues, ensuring effective membrane cleaning [46]. Additionally, these radicals can penetrate the membrane pores, providing comprehensive cleaning.

Optical images of the neat ALO and 450 nm–ZnO/ALO membranes after fouling, backwashing and cleaning steps clearly demonstrate the effectiveness of photocatalytic self-cleansing (Fig. 6c). After each filtration cycle, a thick and compact cake layer of *Scenedesmus* sp. forms on the membrane surface. Following backwashing, the cake layer on the ZnO/ALO membrane is noticeably less dense compared to that on the uncoated ALO membrane. Subsequent rinsing and solar irradiation effectively remove the majority of the deposited biofilm from the ZnO/ALO membrane due to the high AOP activity of the ZnO coating. Any residual deposits on the membrane are minimal and do not impact its filtration performance. In contrast, a significant amount of the biofilm remains on the uncoated ALO membrane after the same procedure. These images, captured after 15 filtration cycles and the backwashing processes, highlight the excellent durability and self-cleaning properties of the ZnO coating on the alumina membrane, ensuring more efficient and sustained performance of the ZnO/ALO membrane over multiple filtration cycles. Table 1 compares the recovery methods and performance of various membrane filtration systems used for microalgae harvesting. The ZnO/ALO membrane demonstrate superior performance, achieving the complete recovery after backwashing and solar irradiation, outperforming most other cleaning methods [26,52,53]. Additionally, the ZnO/ALO membrane offers a straightforward fabrication process and greater durability compared to polymer-based membrane systems [48–51], making it highly competitive among microalgae harvesting systems. This highlights the economic promise of

Table 1
Comparison of flux recovery methods and performance for different microalgae harvesting membrane systems.

Membrane	Microalgae species	Cleaning method	Flux recovery rate (%)	Ref.
ZnO/ALO	*Scenedesmus* sp.	Backwashing + solar irradiation	100%	This work
PVDF/PEI	*Chlorella* sp.	Stirring in water	100%	[48]
PVDF/TA-APTES@FeOOH	*Chlorella vulgaris*	H_2O_2 + solar irradiation	98.2%	[49]
PC@PDA/PEI/PSS/PDADMAC	*Chlorella vulgaris*	Water rinsing	~ 94%	[50]
PVDF	*Chlorella pyrenoidosa*	Water rinsing	90.7%	[51]
Stainless steel	*Chlorella* sp.	NaOH rinsing	68%	[52]
Stainless steel	*Scenedesmus* sp.	Water rinsing + UV irradiation	60%	[26]
Stainless steel	*Microcystis aeruginosa*	Backwashing	39.9%	[53]

using ZnO/ALO membranes for microalgae harvesting. One drawback with the ZnO/ALO membrane is the potential release of by-products, such as Zn^{2+} ions. While these ions can provide health benefits in controlled amounts, excessive release may lead to toxicity risks [54]. Therefore, it is necessary to quantify Zn^{2+} and ROS generated post-treatment and assess their potential impacts on human health. The enhanced self-cleaning properties minimize the need for frequent or prolonged physical cleaning methods, such as vibration, and reduce chemical use. This not only preserves membrane durability but also extends operational lifespan and lowers maintenance costs. This study demonstrates that incorporating a ZnO coating on a ceramic alumina microfiltration membrane is a robust and cost-effective solution for maintaining high membrane performance in microalgae harvesting.

4. Conclusion

ZnO-coated ceramic membranes with self-cleansing capabilities were successfully developed for preconcentrating *Scenedesmus* sp. microalgae prior to harvesting. The ZnO coating enhanced the membrane's hydrophilicity, maintaining high permeate flux despite a reduction in pore size. Results from multiple filtration cycles showed a significant reduction in flux decline for ZnO-coated membranes (200–450 nm thickness) compared to uncoated membranes. However, excessive coating thickness led to pore blockage and reduced efficiency. The optimal 450 nm ZnO coating demonstrated 82% flux recovery after backwashing and rinsing, and 100% flux recovery after 30 min of solar irradiation, minimizing the need for intensive physical or chemical cleaning. Overall, this study presents an antifouling and photocatalytic ZnO-coated membrane filtration system. The approach offers a durable, scalable and cost-effective solution for efficient and sustainable microalgae harvesting, addressing the critical challenges associated with the economic competitiveness of microalgal products.

CRediT authorship contribution statement

Amar K. Salih: Writing – original draft, Visualization, Validation, Methodology, Investigation, Formal analysis, Data curation, Conceptualization. **Curtis P. Irvine:** Methodology. **Fatima Matar:** Methodology. **Lisa Aditya:** Methodology. **Long D. Nghiem:** Writing – review & editing, Supervision, Methodology, Formal analysis. **Cuong Ton-That:** Writing – review & editing, Supervision, Formal analysis.

Declaration of competing interest

The authors declare the following financial interests/personal relationships which may be considered as potential competing interests. Cuong Ton-That reports financial support was provided by Australian Research Council. Cuong Ton-That reports equipment, drugs, or supplies and travel were provided by The Australian Synchrotron. Long D. Nghiem reports a relationship with Journal of Membrane Science that includes: board membership. Long D. Nghiem serves as an Editor of the journal but is not involved in the editorial or review process. If there are other authors, they declare that they have no known competing financial interests or personal relationships that could have appeared to influence the work reported in this paper.

Acknowledgements

This research was partly undertaken on the Soft X-ray Spectroscopy beamline at the Australian Synchrotron, part of ANSTO. The work was supported under Australian Research Council (ARC) Discovery Project funding scheme (project DP210101146). The authors would like to thank Anton Tadich, James Bishop and Herbert Yuan for technical support.

Appendix A. Supplementary data

Supplementary data to this article can be found online at https://doi.org/10.1016/j.memsci.2025.123700.

Data availability

Data will be made available on request.

References

[1] T. Ramachandra, D. Hebbale, Bioethanol from macroalgae: prospects and challenges, Renew. Sust. Energ. 117 (2020) 109479.
[2] N. Kumar, C. Banerjee, J.-S. Chang, P. Shukla, Valorization of wastewater through microalgae as a prospect for generation of biofuel and high-value products, J. Clean. Prod. 362 (2022) 132114.
[3] C. Ju, F. Wang, Y. Huang, Y. Fang, Selective extraction of neutral lipid from wet algae paste and subsequently hydroconversion into renewable jet fuel, Renew. Energy 118 (2018) 521–526.
[4] G. Deviram, T. Mathimani, S. Anto, T.S. Ahamed, D.A. Ananth, A. Pugazhendhi, Applications of microalgal and cyanobacterial biomass on a way to safe, cleaner and a sustainable environment, J. Clean. Prod. 253 (2020) 119770.
[5] L.N. Nguyen, M.T. Vu, H.P. Vu, M.A.H. Johir, L. Labeeuw, P.J. Ralph, T. Mahlia, A. Pandey, R. Sirohi, L.D. Nghiem, Microalgae-based carbon capture and utilization: a critical review on current system developments and biomass utilization, Crit. Rev. Environ. Sci. Technol. 53 (2) (2023) 216–238.
[6] A. Udayan, R. Sirohi, N. Sreekumar, B.-I. Sang, S.J. Sim, Mass cultivation and harvesting of microalgal biomass: current trends and future perspectives, Bioresour. Technol. 344 (2022) 126406.
[7] L. Aditya, H.P. Vu, M.A.H. Johir, S. Mao, A. Ansari, Q. Fu, L.D. Nghiem, Synthesizing cationic polymers and tuning their properties for microalgae harvesting, Sci. Total Environ. 917 (2024) 170423.
[8] I. Demir-Yilmaz, M.S. Ftouhi, S. Balayssac, P. Guiraud, C. Coudret, C. Formosa-Dague, Bubble functionalization in flotation process improve microalgae harvesting, Chem. Eng. J. 452 (2023) 139349.
[9] A. Golzary, S. Imanian, M.A. Abdoli, A. Khodadadi, A. Karbassi, A cost-effective strategy for marine microalgae separation by electro-coagulation–flotation process aimed at bio-crude oil production: optimization and evaluation study, Sep. Purif. Technol. 147 (2015) 156–165.
[10] M. Ghazvini, M. Kavosi, R. Sharma, M. Kim, A review on mechanical-based microalgae harvesting methods for biofuel production, Biomass Bioenergy 158 (2022) 106348.
[11] A. Agarwalla, K. Mohanty, A critical review on the application of membrane technology in microalgal harvesting and extraction of value-added products, Sep. Purif. Technol. (2024) 127180.
[12] J. Zhu, M. Wakisaka, T. Omura, Z. Yang, Y. Yin, W. Fang, Advances in industrial harvesting techniques for edible microalgae: recent insights into sustainable, efficient methods and future directions, J. Clean. Prod. (2024) 140626.
[13] A.K. Lau, M. Bilad, N. Nordin, K. Faungnawakij, T. Narkkun, D.K. Wang, T. Mahlia, J. Jaafar, Effect of membrane properties on tilted panel performance of microalgae biomass filtration for biofuel feedstock, Renew. Sustain. Energy Rev. 120 (2020) 109666.
[14] S. Laksono, I.M. ElSherbiny, S.A. Huber, S. Panglisch, Fouling scenarios in hollow fiber membranes during mini-plant filtration tests and correlation to microalgae-loaded feed characteristics, Chem. Eng. J. 420 (2021) 127723.
[15] L. Aditya, H.P. Vu, L.N. Nguyen, T.I. Mahlia, N.B. Hoang, L.D. Nghiem, Microalgae enrichment for biomass harvesting and water reuse by ceramic microfiltration membranes, J. Membr. Sci. 669 (2023) 121287.
[16] Z. Zhao, B. Liu, A. Ilyas, M. Vanierschot, K. Muylaert, I.F. Vankelecom, Harvesting microalgae using vibrating, negatively charged, patterned polysulfone membranes, J. Membr. Sci. 618 (2021) 118617.
[17] H. Chen, A. Zhou, Y. Zhang, X. Wang, G. Pan, S. Xu, Q. Liu, H. Shan, Q. Fu, J. Ge, Carbonaceous nanofibrous membranes with enhanced superhydrophilicity and underwater superoleophobicity for effective purification of emulsified oily wastewater, Chem. Eng. J. 468 (2023) 143602.
[18] Z.R. Usha, D.M. Babiker, Y. Zhao, X. Chen, L. Li, Advanced super-wetting biaxial polypropylene membrane with hierarchical rough surface for multipollutant removal from oily wastewater, J. Environ. Chem. Eng. 11 (5) (2023) 110775.
[19] J. Lu, T. Bai, D. Wang, H. Yu, Q. Wang, Z. Niu, Y. Hu, X. Liu, G. Han, W. Cheng, Electrospun polyacrylonitrile membrane in situ modified with cellulose nanocrystal anchoring TiO_2 for oily wastewater recovery, Adv. Fiber Mater. 5 (6) (2023) 2055–2068.
[20] N. Daneshvar, D. Salari, A. Khataee, Photocatalytic degradation of azo dye acid red 14 in water on ZnO as an alternative catalyst to TiO_2, J. Photochem. Photobiol., A: Chem 162 (2–3) (2004) 317–322.
[21] K.M. Lee, C.W. Lai, K.S. Ngai, J.C. Juan, Recent developments of zinc oxide based photocatalyst in water treatment technology: a review, Water Res. 88 (2016) 428–448.
[22] Z. Huang, L. Shen, H. Lin, B. Li, C. Chen, Y. Xu, R. Li, M. Zhang, D. Zhao, Fabrication of fibrous MXene nanoribbons (MNRs) membrane with efficient performance for oil-water separation, J. Membr. Sci. 661 (2022) 120949.
[23] J. Yu, L. Zhang, L. Shen, R. Li, D. Zhao, H. Lin, Y. Xu, Y. Jiao, In situ grown cyclodextrin metal-organic framework nanoparticles templated stripe nano-

wrinkled polyamide nanofiltration membranes for efficient desalination and antibiotic removal, J. Membr. Sci. 694 (2024) 122413.
[24] K.-H. Park, P.-F. Sun, E.H. Kang, G.D. Han, B.J. Kim, Y. Jang, S.-H. Lee, J.H. Shim, H.-D. Park, Photocatalytic anti-biofouling performance of nanoporous ceramic membranes treated by atomic layer deposited ZnO, Sep. Purif. Technol. 272 (2021) 118935.
[25] A. Lee, J.A. Libera, R.Z. Waldman, A. Ahmed, J.R. Avila, J.W. Elam, S.B. Darling, Conformal nitrogen-doped TiO_2 photocatalytic coatings for sunlight-activated membranes, Adv. Sustain. Syst. 1 (1–2) (2017).
[26] A.K. Salih, L. Aditya, F. Matar, L.D. Nghiem, C. Ton-That, Improved flux and anti-fouling performance of a photocatalytic ZnO membrane on porous stainless steel substrate for microalgae harvesting, J. Membr. Sci. 694 (2024) 122405.
[27] Z.-Q. Huang, K. Chen, S.-N. Li, X.-T. Yin, Z. Zhang, H.-T. Xu, Effect of ferrosoferric oxide content on the performances of polysulfone–ferrosoferric oxide ultrafiltration membranes, J. Membr. Sci. 315 (1–2) (2008) 164–171.
[28] A. Di Mauro, M. Zimbone, M.E. Fragalà, G. Impellizzeri, Synthesis of ZnO nanofibers by the electrospinning process, Mater. Sci. Semicond. Process. 42 (2016) 98–101.
[29] M. Storms, A.J. Kadhem, S. Xiang, M. Bernards, G.J. Gentile, M.M. Fidalgo de Cortalezzi, Enhancement of the fouling resistance of Zwitterion coated ceramic membranes, Membranes 10 (9) (2020) 210.
[30] R. Goei, T.-T. Lim, Ag-decorated TiO_2 photocatalytic membrane with hierarchical architecture: photocatalytic and anti-bacterial activities, Water Res. 59 (2014) 207–218.
[31] L. Van, M. Hong, J. Ding, Structural and magnetic property of Co-doped–ZnO thin films prepared by pulsed laser deposition, J. Alloys Compd. 449 (1–2) (2008) 207–209.
[32] L.L. Coelho, M. Grao, T. Pomone, M. Ratova, P. Kelly, M. Wilhelm, R.d.F.P. M. Moreira, Photocatalytic microfiltration membranes produced by magnetron sputtering with self-cleaning capabilities, Thin Solid Films 747 (2022) 139143.
[33] R. Vevers, A. Kulkarni, A. Seifert, K. Pöschel, K. Schlenstedt, J. Meier-Haack, L. Mezule, Photocatalytic zinc oxide nanoparticles in antibacterial ultrafiltration membranes for biofouling control, Molecules 29 (6) (2024) 1274.
[34] S. Abou Zeid, Y. Leprince-Wang, Advancements in ZnO-based photocatalysts for water treatment: a comprehensive review, Crystals 14 (7) (2024) 611.
[35] S. Heinonen, J.-P. Nikkanen, E. Huttunen-Saarivirta, E. Levänen, Investigation of long-term chemical stability of structured ZnO films in aqueous solutions of varying conditions, Thin Solid Films 638 (2017) 410–419.
[36] M. Karthik, J.M. Gohil, A.K. Suresh, Probing the thickness and roughness of the functional layer in thin film composite membranes, Int. J. Hydrogen Energy 42 (42) (2017) 26464–26474.
[37] H. Qin, W. Guo, X. Huang, P. Gao, H. Xiao, Nanoscale phase transition seeds-assisted low temperature preparation of α-Al_2O_3 ultrafiltration membrane, Microporous Mesoporous Mater. 293 (2020) 109815.
[38] A. Samavati, H. Nur, A.F. Ismail, Z. Othaman, Radio frequency magnetron sputtered ZnO/SiO_2/glass thin film: role of ZnO thickness on structural and optical properties, J. Alloys Compd. 671 (2016) 170–176.
[39] S. Koonaphapdeelert, K. Li, Preparation and characterization of hydrophobic ceramic hollow fibre membrane, J. Membr. Sci. 291 (1–2) (2007) 70–76.
[40] C.E. Caballero-Güereca, M.A. Cruz, E. Luévano-Hipólito, L.M. Torres-Martínez, Transparent ZnO thin films deposited by dip-coating technique: analyses of their hydrophobic properties, J. Surf. Interfac. 37 (2023) 102705.
[41] K.H. Yoon, H. Kim, Y.-E.K. Lee, N.K. Shrestha, M.M. Sung, UV-enhanced atomic layer deposition of Al_2O_3 thin films at low temperature for gas-diffusion barriers, RSC Adv. 7 (10) (2017) 5601–5609.
[42] M.S. Abdel-Wahab, A. Jilani, I. Yahia, A.A. Al-Ghamdi, Enhanced the photocatalytic activity of Ni-doped ZnO thin films: morphological, optical and XPS analysis, Superlattice. Microst. 94 (2016) 108–118.
[43] L. Miao, C. Wang, J. Hou, P. Wang, J. Qian, S. Dai, Kinetics and equilibrium biosorption of nano-ZnO particles on periphytic biofilm under different environmental conditions, J. Environ. Inform. 23 (2) (2014).
[44] R. Ahmad, J.K. Kim, J.H. Kim, J. Kim, Effect of polymer template on structure and membrane fouling of TiO_2/Al_2O_3 composite membranes for wastewater treatment, J. Ind. Eng. Chem. 57 (2018) 55–63.
[45] P. Prashanth, R. Raveendra, R.H. Krishna, S. Ananda, N. Bhagya, B. Nagabhushana, K. Lingaraju, H.R. Naika, Synthesis, characterizations, antibacterial and photoluminescence studies of solution combustion-derived α-Al_2O_3 nanoparticles, J. Asian Ceram. Soc. 3 (3) (2015) 345–351.
[46] M. Rezayian, V. Niknam, H. Ebrahimzadeh, Oxidative damage and antioxidative system in algae, Toxicol Rep 6 (2019) 1309–1313.
[47] A.K. Salih, M.R. Phillips, C. Ton-That, Enhanced solar-driven water splitting performance using oxygen vacancy rich ZnO photoanodes, Sol. Energy Mater. Sol. Cells 259 (2023) 112436.
[48] T. Hwang, M.R. Kotte, J.-I. Han, Y.-K. Oh, M.S. Diallo, Microalgae recovery by ultrafiltration using novel fouling-resistant PVDF membranes with in situ PEGylated polyethyleneimine particles, Water Res. 73 (2015) 181–192.
[49] Y. Wang, Z. Jiao, W. Li, S. Zeng, J. Deng, M. Wang, L. Ren, Superhydrophilic membrane with photo-Fenton self-cleaning property for effective microalgae anti-fouling, Chin. Chem. Lett. 34 (8) (2023) 108020.
[50] R. Huang, Z. Liu, B. Yan, Y. Li, H. Li, D. Liu, P. Wang, F. Cui, W. Shi, Layer-by-layer assembly of high negatively charged polycarbonate membranes with robust antifouling property for microalgae harvesting, J. Membr. Sci. 595 (2020) 117488.
[51] F. Zhao, X. Han, Z. Shao, Z. Li, Z. Li, D. Chen, Effects of different pore sizes on membrane fouling and their performance in algae harvesting, J. Membr. Sci. 641 (2022) 119916.
[52] A. Ahmad, N.M. Yasin, C. Derek, J. Lim, Chemical cleaning of a cross-flow microfiltration membrane fouled by microalgal biomass, J. Taiwan Inst. Chem. Eng. 45 (1) (2014) 233–241.
[53] D. Xu, Y. Qin, Y. Fang, M. Chen, X. Li, J. Cai, Stainless steel membranes for harvesting cyanobacteria: performance, fouling and cleaning, Bioresour. Technol. 319 (2021) 124143.
[54] S.R. Lee, Critical role of zinc as either an antioxidant or a prooxidant in cellular systems, Oxidative Med, Cell. Longev. 2018 (1) (2018) 9156285.